Taylor & Francis
Taylor & Francis Group

Combustion Theory and Modelling

ISSN: (Print) (Online) Journal homepage: https://www.tandfonline.com/loi/tctm20

Modelling of unsteady pool fires – fuel depth and pan wall effects

H.S. Mukunda, A. Shivakumar & C.S. Bhaskar Dixit

To cite this article: H.S. Mukunda, A. Shivakumar & C.S. Bhaskar Dixit (2021): Modelling of unsteady pool fires – fuel depth and pan wall effects, Combustion Theory and Modelling, DOI: 10.1080/13647830.2021.1980229

To link to this article: https://doi.org/10.1080/13647830.2021.1980229

Published online: 18 Oct 2021.

Combustion Theory and Modelling, 2021
https://doi.org/10.1080/13647830.2021.1980229

Modelling of unsteady pool fires – fuel depth and pan wall effects

H.S. Mukunda, A. Shivakumar* and C.S. Bhaskar Dixit

Fire & Combustion Research Centre, Jain (Deemed-to-be-University), Bangalore, India

(*Received 1 April 2021; accepted 6 September 2021*)

This paper presents physics-inspired mathematical model to predict the time varying burn rate of unsteady pool fires. The model benefits from the observations on the thermal behaviour and select data from systematically and carefully designed experiments on small and large pool fires of n-heptane and small pool fires of diesel, kerosene and ethanol fuels. All modelling features are based on dimensionless quantities. Amongst the three controlling heat transfer mechanisms, convection is dealt with simply. However, conduction and radiant heat transfer models have needed new considerations. A combination of steady and unsteady conduction along the pan wall affected by the thermal properties of the wall material and liquid phase conduction are modelled and validated against specific experiments. Radiant heat transfer modelling differs from the conventional approach to account for fuel depth-dependent enhancement in burn flux in small pans to values comparable to large pool fires. The radiation view factor invokes mass flux based Reynolds number to account for fuel depth-related effects. Several constants are modelled in terms of dimensionless parameters constructed from a large number of physical variables of the pan and the fuel and used in the model such that they allow the best fits between the simulation and a part of the experimental data. All the sub-models combined into a surface heat flux balance provide the temporal variation of the mass depletion as also the relative magnitudes of the fluxes in a MATLAB code. Comparisons of the predictions on the dependence of the burn behaviour on fuel depth, free board, pan diameter and wall material with the experimental data of the present authors and from literature on n-heptane are set out. Comparisons between the predictions and experimental data on diesel, kerosene and ethanol are also set out to show the ability of the model to track the mass loss history based on fundamental properties of the fuel and the pan. The outstanding-to-good quality of predictions in most cases is attributed to the necessary physics taken into account in the model.

Keywords: pan fire; pool fire modelling; unsteady pan fire model

List of Symbols

English Symbols

A_1		Cross-sectional area (m)
c_{pw},	c_{pfu}	Specific heat of wall material and fuel (kJ/kg K)
c_{Tp}		Coefficient used in Pan tip temperature calculation (Equation (25))
C_{21}, C_{22}		Constants used in determining types I/II (Equations (33) and (34))
C_3		Constant used in determining types I/II (Equation (36))
d_{pan}		Pan diameter (m)

*Corresponding author. Email: shivakumarannaiappa@gmail.com

evf	Product of constant part of emissivity and view factor
ff	Correction factor of pan size effects on radiation (Equation (13))
h_{pan}, h_{fu}, h_{fb}	Pan and fuel depths and Freeboard (m)
$h_{\text{g,conv}}$	Gas phase convective heat transfer coefficient (kW/m^2 K)
h_{gcv0}	Initial gas phase convective heat transfer coefficient (kW/m^2 K)
$h_{g,ft}$	Gas phase heat transfer coefficient near wall tip (kW/m^2 K)
$h_{g-w,fu}$	Heat transfer coefficient from the wall to the liquid (kW/m^2 K)
L_{fu}	Latent heat of vapourisation of the fuel (kJ/kg)
k_w	Thermal Conductivity of pan wall material (kW/m K)
k_{fu}	Thermal Conductivity of fuel (kW/m K)
$\bar{m}''_{\text{fu}}$	Mean burn flux (kg/m^2 s)
M_{pc}	Dimensionless pan burn number (Equation (5))
$Mpc1$	Dimensionless number to distinguish types I and II (Equation (27))
p	Pressure in atm
$\dot{q}''$	Heat flux (kW/m^2)
$\dot{r}$	Fuel regression rate (m/s)
S	Stoichiometric Ratio
T	Temperature (K)
T_0	Initial temperature of the liquid fuel (K)
T_{bot}	Bottom temperature in the liquid pool (K)
W	Dimensionless number to capture behaviour of T_p (Equation (23))
$W1$	Dimensionless number to calculate C_3 (Equation (36))

Greek Symbols

α_{fu}	Thermal diffusivity of fuel (m^2/s)
ϵ	Emissivity
κ_{ex}	Extinction coefficient (1/m)
η_{fu}	Dimensionless distance-into-fuel coordinate (Equation (37))
ρ_{fu}	Density of fuel (kg/m^3)
σ	Stefan–Boltzmann constant (W/m^2 K^4)

Subscripts

conv, cond	Convection, Conduction
rad, tot	Radiation, Total
p, pm	Pan tip, Steady pan tip
s, f	Surface, Flame
wb, wbc	Pan bottom outer wall, pan bottom central zone

1. Introduction

The modelling of pool fire gained importance with the publication of a review of Russian work on pan fire by Hottel [1]. Prediction of the burn rate invokes the surface heat balance [2, 3] as in Equation (1)

$$\rho_{\text{fu}} \dot{r} H_s = \dot{q}''_{g,\text{conv}} + \dot{q}''_{g,\text{rad}} + \dot{q}''_{\text{wall cond}} \tag{1}$$

Where the left-hand side is the flux demanded for vapourisation with heat of phase transformation being H_s, the three terms on the right-hand side refer to heat fluxes received from the gas phase via convection, radiation and wall conduction. While the steady-state models can justifiably ignore wall conduction, the fixed fuel pan based burn process has to include it. Spinti et al. [2] have brought out the known heat balance basis of models described earlier by Hamins et al. [3], but no predictions from the models are presented. Several investigators [4–7] have presented models for predicting the burn flux from pan fires.

Ndubizu et al. [4] consider a pan with liquid filled to the top. Wall heat transfer and fuel depth are not considered in the treatment. The temperature of the fire is related to the amount of air entrained into the fire due to buoyancy and a complex set of relations involving the air-to-fuel ratio are solved. The solution turns out to be very sensitive to the air-to-fuel ratio. The unknown in terms of flame temperature is transferred to air-to-fuel ratio and it is not clear if this can be determined accurately either. The radiation model treats extinction coefficient as set out in Equation (2) which has become a standard approach described in Babrauskas [8]. In fact, most published work in the area of fires uses Equation (2).

$$\dot{q}''_{g,\mathrm{rad}} = v_F \epsilon \sigma T_f^4 [1 - \exp(\kappa_{\mathrm{ex}} d_{\mathrm{pan}})] \tag{2}$$

where v_F is the view factor, ϵ is the emissivity, σ is the Boltzmann constant, T_f, the flame temperature, κ_{ex} is the extinction coefficient and d_{pan} is the pan diameter. The data on the estimate of the extinction coefficient is set out in a table in Babrauskas [8]. While the values of the extinction coefficient for fuels like methanol and ethanol are much lower than for hydrocarbons, the values for various hydrocarbons, either are not available or where available, very difficult to rationalise. This is understandable since it depends on the composition of the very fuel-rich reaction zone above the fuel surface and the processes of pyrolysis and reaction under rich conditions are very complex, particularly in the buoyant turbulent flow. In more recent experimental study, Chatris et al. [9] and Munoz et al. [10] evaluate the extinction coefficients for diesel and gasoline fire tests that they have presented and come up with values that differ from earlier literature by orders of magnitude. For instance, Babrauskas [8] has deduced values of κ of 1.6–3.6 for petroleum fuels, Chatris et al. [9] provide a table with values by various authors, their own value for κ is 0.57 for diesel and 1.35 for gasoline. This range of values implies that fits are dependent on specific data and rationalisation calls for inclusion of all dependent parameters.

While de Ris and Orloff [5] presented in an early study a correlation for the burn flux in terms of transfer number, B with limited value, subsequently, Orloff and de Ris [6] have presented a model for estimating the burn flux of moderate pool fires (0.1 –0.7 m dia) using a procedure that invokes approximations to flame structure and estimation of radiation flux with an extinction coefficient based on a curve fit that is expected to be very accurate (in fact, the coefficients have five to six significant digits). However, they choose a fixed value of 1200 K as the flame temperature, T_f. If we recognise that T_f appears in terms of fourth power, any small errors in the choice can result in gross errors in the prediction of the heat fluxes and so, burn flux as well.

Ditch et al. [7] have pursued producing an empirical correlation over a large number of fuels – many of them synthetic to create a range of fuels with different properties controlling the steady burn rate. Equation (2) is still the basis of their correlation. The extinction coefficient is related to the volume of heat release, the radiant fraction and combustion

efficiency and the modifications made to the heat flux reads as

$$\dot{m}'' H_s = 12.5 + 68.3 Y_s^{0.25} \left[1 - \exp\left[-(4/3) H_s {d_{\text{pan}}}^{3/2}\right]\right] \tag{3}$$

where $H_s = [L_{\text{fu}} + c_{p,fu}(T_s - T_0)]$, H_s is the heat of gasification, L_{fu} is the latent heat of vapourisation, Y_s is the smoke point of the fuel. The key parameters in the model are the heat of gasification and smoke point of the fuel. The correlation is shown to work well for many fuels. In the above equation, the value 12.5 on the right-hand side refers to the convective flux from the gas phase and when added to 68.3 $Y_s^{0.25}$ the large pan size burn flux close to 80 kW/m^2 will result. While the aim of obtaining the equation has been to eliminate the lack of a procedure to determine the extinction coefficient, the fact that only dimensional quantities are used in the exponential term of the above equation indicates to the fact that the physics has not been captured completely. They [7] also quote the results of Li et al. [11] and Fang et al. [12] and appear concerned by the large differences between the results in unsteady burn flux in these two experimental studies. Both these studies [11, 12] have pointed out that the differences in their results are because convective and radiative fluxes are dependent on pressure and they have rationalised their results based on the pressure effect that has been studied earlier by de Ris et al. [13] and invoked by Weiser et al. [14] and Alpert [15]. In their paper, de Ris et al. [13] present scaling arguments that show that both convective flux and radiation flux scale as $p^{2/3}$, where p is the pressure in atm.

Even with a reasonable broad understanding of the relative roles of convection and radiation on pan fires, there are many unresolved aspects that need examination. Apart from conduction that needs careful modelling to rationalise the results with different pan materials and pan sizes from small to large, expressions for radiation flux merit reconsideration since (a) the expression for radiation flux as modified by Ditch et al. [7] perhaps is not even rightly scaled because it is not dimensionless and (b) the results on pressure effect in Refs. [11, 12] brought out in [7] still remain unaddressed.

In the background of several points made above, a systematic experimental study was conducted by the present authors on pans of different materials with n-heptane fuel (glass, stainless steel, mild steel and aluminum) for small pans -0.2 m diameter, pans of mild steel with different sizes (0.2, 0.3, 0.4, 0.5, 1 and 2 m diameter) in Shiva kumar et al. [16] and experiments with diesel, kerosene and ethanol fuels were conducted in 0.2 m diameter pans in Shiva kumar et al. [17]. Data on mass burn, wall temperatures and in-depth liquid temperatures as a function of time were obtained and the data were correlated for the mean burn fluxes as a function of dimensionless parameters to account for geometric, thermodynamic and thermo-chemical variables.

The expression for the steady burn flux is

$$\bar{\dot{m}}''_{\text{fu}}(g/m^2 s) = M_{pc} \frac{h_{\text{g,conv}}(T_f - T_{bfu})}{4 L_{\text{fu}}} \tag{4}$$

Where M_{pc} is set out as

$$M_{pc} = P_1 P_3 [1.5 + 8.5 P_2] \quad \text{with} \tag{5}$$

$$P_1 = \left[\frac{k_w}{h_{\text{pan}} h_{\text{g,conv}}} \frac{h_{\text{fu}}}{h_{fb}}\right]^{1/4} \tag{6}$$

$$P_2 = \left[1 - \exp(-0.25 (d_{\text{pan}}/0.21)^{1.5}/P_1)\right]\left[1 + 0.1 (h_{wr}/h_{\text{pan}})^{2.3}\right] \tag{7}$$

$$P_3 = \left[\frac{(T_{bfu} - T_0)}{(T_{bfu} - 300)}\frac{300}{T_{bfu}}\right]^{-0.35} \tag{8}$$

The parameter P_1 accounts for conductive flux in addition to fuel depth and associated freeboard effects, P_2 accounts for the effect of pan diameter and water on the mass burn rate and P_3 for initial temperature effects. The above correlation has been found to be correct to less than a mean of 5% for both unsteady and steady experiments over a wide range of parameters [16,17].

The present effort is to progress on this work to predict the mass burn as a function of time through modelling of convection, conduction and radiation.

2. Elements of the new model

It has been known that the heat flux balance is the basis of burn rate prediction as in Equation (1). In the first term is given by H_s is given by $[L_{\text{fu}} + c_{p,fu}(T_s - T_{\text{bot}})]$ where T_s and T_{bot} are the surface and the bottom layer temperature of the fuel. Fuel surface temperature can be set as ambient temperature or of heated fuel as in the case of Chen et al. [18]. The bottom layer temperature is also the initial set temperature, but changes with time because of heat transfer from the surface. The second, third and fourth terms are explained below. The in-depth radiant heat absorption by the fuel and the loss due to re-radiation from the pool surface are small compared to the heat flux received at the surface by radiation. They act in opposite directions and are together neglected. This is consistent with the approach chosen in Ditch et al. [7].

2.1. *Convection term*

The second term with respect to heat flux from gas phase has two components – convection and radiation. The convective flux, is given by

$$\dot{q}''_{\text{conv}} = h_{\text{g,conv}}(T_f - T_s) \tag{9}$$

With regard to the gas phase heat transfer coefficient, $h_{\text{g,conv}}$, it was determined from the experimental data across all diameters and wall materials, that there is an initial phase of mass loss vs. time that can be predicted well with a value of $0.0045\,\text{kW/m}^2K$. This inference was obtained by examining the experimental data of n-heptane over all the cases in 0.2 m diameter cases (and in the case of other fuels like kerosene and diesel). This was found satisfactory for all experiments at ambient pressure of about 1 atm. Experiments by Li et al. [11] and Fang et al. [12] at very different altitudes showed a pressure dependence of the pan fires and has been a subject of studies [13–15] as brought out earlier. The pressure dependence drawn from Ref. [13] is taken to give

$$h_{g,\text{conv}} = 0.0045p^{2/3} \tag{10}$$

2.2. *Gas phase radiation*

The radiation model deployed here is different in its elements compared to those used in literature and is a consequence of the results of the experiments that have shown that the mass flux from smaller diameter pans (~ 0.2 m) can become as large as larger pans when

larger depths of fuel are involved [16]. The fact that the flux can increase significantly due to fuel vapourisation processes controlled by wall conduction (discussed below) has to be accounted for to explain much higher burn rates in smaller diameter pans. The increase in the burn flux is so large with values comparable to large pool fires that conduction alone was found inadequate to explain the results. Also, when the pan diameter increases from about 0.2 m considered small, through larger values up to 2 m and at different fuel thicknesses, it was found imperative to invoke a dependence due to enhanced burn flux at small diameters. To introduce dimensionless approach, a Reynolds number based on fuel mass flux and pan diameter is invoked. The diameter dependence is also brought into account for flame emissivity coupled with changes in view factor. Further, accounting for pressure dependence is performed based on [13]. Therefore, radiation flux is expressed as

$$\dot{q}''_{\text{rad}} = p^{2/3} evf\, \sigma T_f^4 \quad \text{with} \tag{11}$$

$$evf = 0.2\left[1 - e^{-0.00045 ff \frac{\bar{m}''_{\text{fu}} d_{\text{pan}}}{\mu_g}}\right] \quad \text{and} \tag{12}$$

$$ff = 1 - e^{[-0.4(d_{\text{pan}}/0.21)^3]} \tag{13}$$

where 'evf' is the product of the constant part of emissivity and view factor and ff is a further correction to pan size effects on radiation, determined after comparing with radiation effects at fixed fuel thickness over a range of pan diameters. In the expression for evf, the increase in radiant flux expected due to enhanced flame height because of the need to account for larger fuel depths. The value of 0.2 in the expression for evf is a constant that has been determined to get good comparison of the mass vs. time for 0.2 and 2 m diameter pans and remains unchanged. In ff, d_{pan} can be understood to be rendered dimensionless by 0.21 m instead of $[\nu_g^2/g]^{1/3}$ which is close to this value depending on the choice of the temperature for evaluating the kinematic viscosity. The above correlation was shown to give a mean error less than 5% over a wide range of parameters.

2.3. *Wall conduction to fuel*

The third term related to wall conduction is modelled using the heat flux balance at the pan edge. This model is elaborate and has several models were attempted before arriving at the following approach. It is conceived that the top region (constituting a region of the order of the thickness of the pan) has a temperature, T_p and the heat transfer occurs from the flame with temperature T_f that moves down the pan wall by conduction. The difference in the heat flow will raise T_p over a time. The heat balance equation is

$$m_w c_{pw} t_w \frac{\mathrm{d}T_p}{\mathrm{d}t} = h_{g,ft}(T_f - T_p)A_1 - h_m(T_p - T_0)A_1 \tag{14}$$

where m_w, c_{pw}, t_w and A_1 refer to mass, specific heat, wall thickness and the cross section – $\pi d_{\text{pan}} t_w$, $h_{g,ft}$ is the gas phase heat transfer coefficient near the wall tip and h_m, the wall heat transfer coefficient. It is defined by the ratio of $k_w/(h_{ft} +$ fuel regression). Fuel regression, reg is obtained as $\int_0^t \dot{r}\mathrm{d}t$ with $\dot{r}$ being the linear regression rate of the fuel. We can recast Equation (14) as

$$\frac{\mathrm{d}T_p}{\mathrm{d}t} = \frac{h_{g,ft}}{\rho_w t_w c_{p,w}}\left[(T_f - T_p) - \frac{h_m}{h_{g,ft}}(T_p - T_0)\right] \tag{15}$$

At $t = 0$, since $T_p = T_0$, we get

$$\frac{\mathrm{d}T_p}{\mathrm{d}t}]_{t=0} = \frac{h_{g,ft}}{\rho_w t_w c_{p,w}}(T_f - T_0) \tag{16}$$

From the experimental data on T_p vs. time [16] shows that $\mathrm{d}T_p/\mathrm{d}t]_{t=0}$ is around 2.8 K/s independent of the material of the pan. We denote $\mathrm{d}T_p/\mathrm{d}t]_{t=0}$ by G (= 2.8 K/s). We express h_m by $k_w/(h_{fb} + reg)$ and write

$$\frac{\mathrm{d}T_p}{\mathrm{d}t} = G\left[\frac{T_f - T_p}{T_f - T_0} - \frac{k_m}{h_{\mathrm{pan}} h_{g,ft}} \frac{h_{\mathrm{pan}}}{h_{fb} + reg} \frac{T_p - T_0}{T_f - T_0}\right] \tag{17}$$

The quantity $k_m/(h_{\mathrm{pan}} h_{g,ft})$ is denoted by c_{Tp} and is a constant whose parametric dependence of various quantities must be determined yet. Thus the final form of the equation for T_p is

$$\frac{\mathrm{d}T_p}{\mathrm{d}t} = G\left[\frac{T_f - T_p}{T_f - T_0} - c_{Tp} \frac{h_{\mathrm{pan}}}{h_{fb} + reg} \frac{T_p - T_0}{T_f - T_0}\right] \tag{18}$$

The distribution of the wall temperature from the tip to the bottom wall centre needs to be described. The temperature distribution along the radius of the circular pan bottom still be a constant value if it is steady (because the steady solution in a cylindrical geometry leads to this result). However, experimental data involving a thermocouple mounted at the bottom wall centre shows an increase in temperature [16], in fact close to the liquid temperature next to the wall. In view of this finding, it is taken that the linear heat transfer drop to the central region defined as a circular part of radius $= d_{\mathrm{pan}}/4$ will heat up this region with time. This assumption leads to

$$\rho_w c_{pw} \pi (d_{\mathrm{pan}}/4)^2 t_w \frac{T_{wbc}}{\mathrm{d}t} = \frac{k_w}{(h_{\mathrm{pan}} + d_{\mathrm{pan}}/4)}(T_p - T_{wbc}) \pi d_{\mathrm{pan}} t_w \tag{19}$$

where T_{wbc} is the temperature in the bottom central zone of a diameter $= d_{\mathrm{pan}}/2$. This equation can be recast as

$$\frac{T_{wbc}}{\mathrm{d}t} = \frac{k_w}{(h_{\mathrm{pan}} + d_{\mathrm{pan}}/4)} \frac{16}{\rho_w c_{pw} d_{\mathrm{pan}}}(T_p - T_{wbc}) \tag{20}$$

This equation is solved numerically along with other equations since T_p is also a function of time. The heat transferred to the liquid is computed using two temperatures, T_{w1} and T_{wb}, the values at the position of the liquid layer and at the bottom of the edge of the pan, essentially to obtain a better estimate of the heat transfer.

Using linear temperature drop along the wall as found to be approximately true from the experiments [16], we can set

$$T_{w1} = T_p - (T_p - T_{wbc}) \frac{h_{fb} + reg}{h_{\mathrm{pan}} + d_{\mathrm{pan}}/4} \tag{21}$$

$$T_{wb} = T_p - (T_p - T_{wbc}) \frac{h_{\mathrm{pan}}}{h_{\mathrm{pan}} + d_{\mathrm{pan}}/4} \tag{22}$$

We need to device a method to determine c_{Tp} to complete the predictive scheme. For this purpose, it is intended to seek the connection between the steady maximum tip temperature value of T_p, identified as T_{pm} and various parameters for which experiments have been

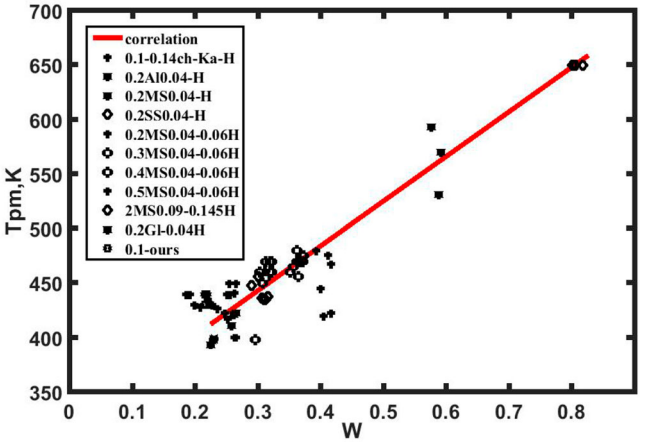

Figure 1. Variation of steady maximum wall tip temperature, T_{pm} with a dimensionless parameter, W (*0.2MS0.04-0.06H, implies 0.2* m *diameter mild steel pans of 0.04–0.06* m *depth with n-heptane fuel*).

conducted. The values of T_{pm} are the lowest for aluminum (just above the boiling point of n-heptane) and very high for glass and moderate for small pan diameters and very high for large diameters [16], essentially because of the thermal conductivity (as also the thermal diffusivity) of the materials. A new dimensional number W is constructed to obtain a *monotonic behaviour* of steady pan tip temperature with the various parameters considered in the experiments and is defined as

$$W = \left[\frac{d_{\text{pan}} h_{gcv0}}{k_w}\right]^{0.5} d_{\text{pan}}^{0.25} \left[\frac{h_{\text{fu}} h_{fb}}{h_{\text{pan}}^2}\right]^{0.1} \left[\frac{T_{bfu}}{T_0}\right]^{0.5} \tag{23}$$

The choice of the various terms needs description. The first term on the right-hand side of the equation accounts for conductive and convective flux using d_{pan} as the characteristic dimension instead of h_{pan} as is the case with M_{pc}, the last term accounts for fuel initial temperature effects as in the case of M_{pc}. The third term with a small exponent was introduced to take into account the effect of free board in conjunction with fuel depth and the parameter d_{pan} in $d_{\text{pan}}^{0.25}$ should be understood to be rendered dimensionless by a constant $[\nu_g^2/g]^{(1/3)}$. Since this is not introduced into the equation, expressing d_{pan} in SI units would be appropriate. It must be understood that the development of the parameter W took place in stages after determining the strongest influences first and moving towards smaller influences trying to preserve the monotonicity of the behaviour as set out in Figure 1. Though several points at small W showed deviations, these did not reflect in the overall behaviour of the mass loss vs. time predictions. The expression for T_{pm} vs. W becomes

$$T_{pm} = 320 + 410W \tag{24}$$

Having calculated T_{pm}, we can get c_{Tp} from

$$c_{Tp} = \frac{T_f - T_{pm}}{T_{pm} - T_0} \tag{25}$$

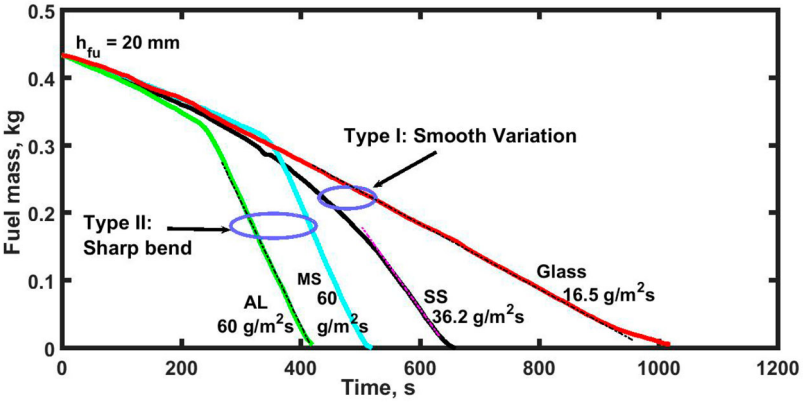

Figure 2. Burn mass vs. time for a 200 mm pan with 3 mm wall thickness with different pan materials.

The conductive heat transferred to the liquid is taken as

$$\dot{q}''_{\text{cond}} = h_{g-w,fu}\left[(T_{wb} - T_{\text{bot}}) + 4\frac{(h_{\text{fu}} - reg)}{d_{\text{pan}}}[(T_{w1} + T_{wb})/2 - (T_s + T_{\text{bot}})/2]\right] \quad (26)$$

where $h_{g-w,fu}$ is the heat transfer coefficient from the wall to the liquid, T_{bot} is the liquid bottom temperature and T_s is the liquid surface temperature, both treated uniform over the diameter and are determined from conduction analysis to be discussed below. In the above equation, the first term in the parenthesis corresponds to heat transfer from the pan bottom to the liquid and the second term to the heat transfer from the sides to the liquid. For the latter term, an average of temperatures is taken even though there may be other equivalent ways of accounting for heat transfer. It is necessary to describe the approach to determine the pan wall heat transfer coefficient $h_{g-w,fu}$. At this stage, it is important to examine the effect of different pan materials on the burn behaviour in small diameter pans. Figure 2 shows the mass vs. time for different materials for a 200 mm diameter pan. It can be noted that aluminum and mild steel pans exhibit a sharp change in slope (identified as type II) unlike stainless steel and glass that show a smooth behaviour (identified as type I). Experiments at fuel temperature close the boiling point also exhibited such a behaviour while all other experiments showed smooth variation (type I), even in the large diameter MS pans. The reason for such different behaviour in AL and MS pans is due to increased conduction heat transfer rate in small pans. To account this behaviour and obtain predictive procedure over a wide range of geometric and thermo-chemical parameters, it was thought necessary to classify them using dimensionless quantities. After a detailed examination, it was found that it would be necessary to invoke a non-dimensional number $Mpc1$ as follows.

$$Mpc1 = \left[\frac{k_w}{h_{\text{pan}}h_{gcv0}}\right]\left[\frac{4t_w}{d_{\text{pan}}}\right]\left[\frac{h_{\text{fu}}}{h_{\text{pan}}}\frac{L_{\text{fu}}}{c_{pfu}(T_{bfu} - T_0)}\right]^{0.25}\left[1 - 0.3(h_{\text{pan}}/d_{\text{pan}})^{0.125}\right] \quad (27)$$

The first term on the right-hand side of the equation accounts for the conductive flux scaled with the convective flux, again as in the case of M_{pc}, second and fourth terms account for the pan wall thickness and pan depth effects and the third term accounts for the fuel depth

and fuel properties effect. With this parameter, the wall heat transfer coefficient is set out as

$$h_{g-w,fu} = h_{\mathrm{g,conv}}, for\ Mpc1 < 1 \tag{28}$$

$$h_{g-w,fu} = S_l, for\ Mpc1 > 6.5\ \&\ m_{\mathrm{fu}}/m_0 < C_2 \tag{29}$$

$$h_{g-w,fu} = h_{\mathrm{g,conv}}\left[1 + C_3\frac{reg}{h_{\mathrm{fu}}}\right], \quad for \quad Mpc1 > 1\ \&\ Mpc1 \leq 6.5 \tag{30}$$

The constants C_2 and S_l are chosen for best fits to a few cases of the simulation and seeking good comparison with experimental data. For cases with sharp variation in mass vs. time behaviour (type II),

$$S_l = 0.1Mpc1 - 0.26 - 0.0017(Mpc1)^2 \quad \text{for} \quad 6.5 < Mpc1 < 10 \tag{31}$$

$$S_l 0.45 \quad \text{for}\ Mpc1 > 10 \tag{32}$$

The specific values in the above expressions were determined after testing the code with changes in the values noted above to get a good fit for the variation with time on a few cases. The value of constant C_2 is obtained as

$$C_2 = 0.6 + 0.0575(Mpc1 - 6) \quad \text{for} \quad 6.5 < Mpc1 < 10 \tag{33}$$

$$= 0.83 - 0.3(Mpc1^{0.25} - 1.78)/Mpc1^{0.25} \quad \text{for} \quad \mathrm{Mpc1} > 10 \tag{34}$$

In order to determine C_3, calculations were made on several cases using the pan burn code (to be described below) to determine the value of C_3 that gives the best fit of mass loss vs. time data for specific cases. The variation of C_3 with different parameters and possible dimensionless quantities that could be conceived from these parameters to seek a consistent and smooth behaviour was attempted. These needed the evolution of a new parameter, W_1 defined below.

$$W_1 = \frac{1}{222}\left[\frac{k_w}{h_{fb}h_{gcv0}}\right]^{0.5}\left[\frac{h_{\mathrm{pan}}}{d_{\mathrm{pan}}}\right]^{0.5}\left[\frac{T_{bfu}}{T_0} - 1\right]^{0.25} \tag{35}$$

Here again, the choice of the variables in the terms within the brackets followed the same procedure for W and M_{pc1}. With this parameter, C_3 is obtained from

$$C_3 = 2200(W_1 - 0.026) \tag{36}$$

Thus the conduction modelling that is very important for small and medium sized pans (< 1 m diameter) and the constants needed to get good comparisons with experimental data are T_{pm}, C_2, S_l and C_3. These are related to dimensionless quantities W, $Mpc1$ and W_1. The choice of the properties of fuel and pan wall materials, and conditions of operation (like the fuel temperature) control these parameters. There are *no adjustable constants* in the model.

2.4. *Liquid phase conduction*

The heat transfer process inside the liquid is taken to be conduction only. This inference is arrived at by first noting that since the liquid in-depth is always at a lower temperature, there will be no upward natural convection and then the results of the experiments by Ditch et al. [7] where it was shown that the presence or the absence of glass beads below

the surface has little influence on the burn rate of steady combustion process. Further, Chen et al. [19] have performed their unsteady analysis taking only conduction process as relevant.

There are two aspects to the liquid phase conduction process. The increase of surface temperature with time and the conduction process through the fuel or fuel-on water. We consider the conduction process first. Transient conduction process is governed by the dimensionless quantity $y/\sqrt{\alpha_{\rm fu} t}$ where $\alpha_{\rm fu} = k_{\rm fu}/(\rho_{\rm fu} c_{p,fu})$ is the thermal diffusivity of the fuel. Since the fuel is regressing, y distance into the liquid is replaced by $y - \int \dot{r} {\rm d}t$. The temperature at any location inside the fuel is given by $(T - T_{\rm bot})/(T_s - T_{\rm bot})$ being a function of a dimensionless coordinate $(y - \int \dot{r} {\rm d}t)/\sqrt{\alpha_{\rm fu} t}$. It has been taken as

$$\frac{T - T_{\rm bot}}{T_s - T_{\rm bot}} = \exp[-C_4 \eta_{\rm fu}^m] \quad \text{where} \quad \eta_{\rm fu} = \frac{(y - \int \dot{r} {\rm d}t)}{\sqrt{\alpha_{\rm fu} t}} \tag{37}$$

Temperatures measured inside n-heptane fuel in the experiments of Chen et al. [18] and one experiment from this laboratory were chosen for exploring the validity of the above expression. Amongst various choices, it turned out that $m = 0.66$ gave a fit with a linear behaviour up to a point when the temperature reached near-boiling point. Data on liquid temperatures at various depths from Chen et al. [18, 19] and fuel–water interface temperature from an experiment on 500 mm pan with 30 mm heptane and 20 mm water is shown in Figure 3. In the plot $\alpha_{\rm fu}$, the thermal diffusivity of heptane is taken as 0.09 mm^2/s. As can be noted all of the data collapse on a single line for the chosen coordinate. The temperature profile can therefore be summarised as

$$(T - T_{\rm bot}) = 3(T_s - T_{\rm bot}) \exp[-\eta_{\rm fu}^{0.66}] \quad \text{for} \quad 0 < \eta_{\rm fu} < 0.33 \tag{38}$$

Beyond a value of $\eta_{\rm fu} > 0.33$, boiling point is reached. The result for 30 mm heptane and 20 mm water departs from the linear behaviour in Figure 3 due to the role of water close to the boiling point. We need to consider the variation of the surface temperature to reach the boiling point. Surface temperature increases because the difference between the heat flux from the gas phase and the heat flux due to conduction into the liquid raising the temperature of the liquid layer. While classically, this is treated using Clausius–Clapeyron equation (see [20]) assuming *equilibrium at the surface*, in the current approach, it is treated as *a rate process* in which the enthalpy rise rate of the surface layer of thickness, δ_l equals the differences in the fluxes between the gas phase and liquid phase. The flux into the liquid $\dot{q}_l'' = k_{\rm fu} {\rm d}T_s/{\rm d}y$ at $(y - \int \dot{r} {\rm d}t) = \delta_l$ is obtained as

$$\left[k_{\rm fu} \frac{{\rm d}T_s}{{\rm d}y} \right]_{\delta_l} = \dot{q}_l'' = 3 k_{\rm fu} (T_s - T_{\rm bot}) G_l \tag{39}$$

$$G_l = \frac{0.66 \exp[-\eta_l^{0.66}]}{\delta_l^{0.34} (\sqrt{\alpha_{\rm fu} t})^{0.66}} \tag{40}$$

The gradient is taken at a depth of δ_l into the surface to avoid singularity. Here $\eta_l = \delta_l/\sqrt{\alpha_{\rm fu} t}$. The heat balance at the surface becomes

$$\rho_{\rm fu} c_{p,fu} \delta_l \frac{{\rm d}T_s}{{\rm d}t} = \dot{q}_{tot}'' - \dot{q}_l'' \tag{41}$$

The value of δ_l is chosen so as to replicate the surface temperature rise in one experiment. The data of Chen et al. [18] are used for this purpose.

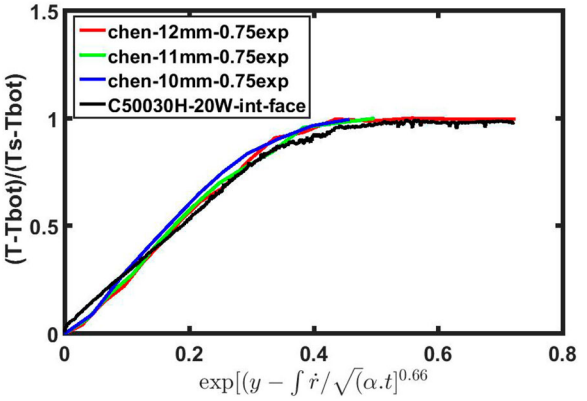

Figure 3. Centreline temperatures inside the liquid for heptane pool fire in 200 mm dia pan [16] and the heptane–water interface temperature for 30 mm heptane and 20 mm water [18] on dimensionless coordinates.

Table 1. Properties of pan ($t_{\text{cond}} \sim h_{\text{pan}}^2/4\alpha_w/2$) [16].

Material	d_{pan} mm	t_w mm	ρ_w kg/m^3	c_{pw} kJ/kg K	k_w W/m K	α_w mm^2/s	h_{pan} mm
Al	200	3	2730	0.91	60	24.1	40
MS	200	3	7800	0.46	32	8.9	40–60
SS	200	3	7800	0.46	16	4.45	40–60
SS [19]	200	3	7830	0.48	21	5.6	40
Glass	190	3	2230	0.75	1.14	0.68	40

3. Data on properties

In carrying out the calculations, one would need the thermal properties of the pan materials. These are set out in Table 1. The fuel properties are set out in Table 2. The properties are drawn from standard data sources and two fuels, namely, kerosene and diesel need discussion. Since both kerosene and diesel constitute a mix of several fractions of compounds that are soluble with each other with different boiling points, the issue of the choice of the boiling point (T_{bfu}) and latent heat of vaporisation (L_{fu}) were critically examined in the light of the studies reported by Spinti et al. [2]. To the extent that the simulation should predict the mass loss-time data, the choice of these parameters was made such that they would predict the mass loss data as well as possible. The choice of these values for the boiling point were found to be in the boiling range of these fuels. With regard to the flame temperature measurements were made using K-type thermocouple of bead size of 0.4 mm. The detailed procedure adopted to measure the flame temperature is discussed in reference [16]. In order to measure the temperature, beads were made red hot in a blue LPG-air flame and then immediately introduced into the flame to ensure that soot deposits do not affect the measured data. The flame temperatures are shown in Figure 4. Table 2 also shows data on flame temperatures measured by other investigators [21, 22] in case of diesel and ethanol. The measured values are in close agreement with the values reported in the literature. The gas phase-specific heat and viscosity are taken as $c_{p,g} = 1.0$ kJ/kg K, $\mu_g = 1.8 \times 10^{-5}$ kg/m s.

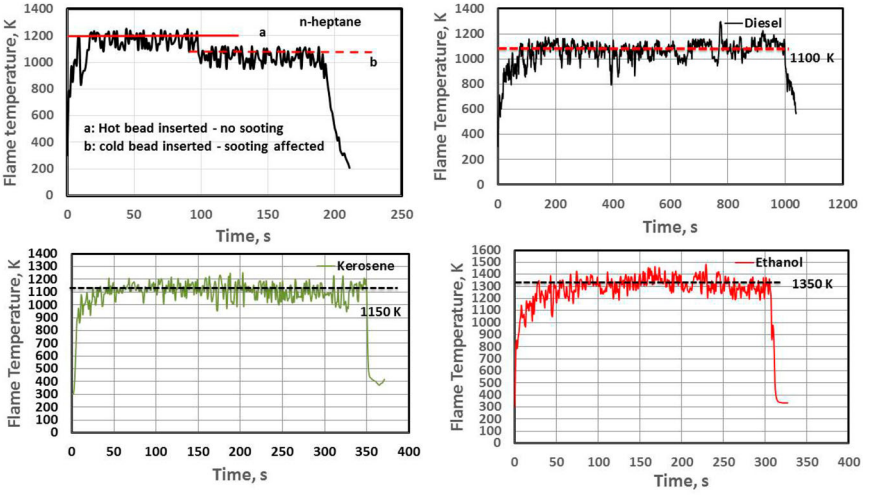

Figure 4. Centreline flame temperature at a height of 0.4 dpan vs. time for n-heptane, diesel, kerosene and ethanol fuels in 0.2 m diameter pool fire.

Table 2. Properties of the fuel [16].

Fuel	ρ_{fu} kg/m^3	T_{bfu} K	c_{pfu} kJ/kg K	L_{fu} kJ/kg	k_{fu} W/m K	α_{fu} mm^2/s	μ_{fu} mN s/m^2	T_f K
n-heptane	680	369	2.1	322	0.14	0.090	0.409	1200
Kerosene	810	490	2.01	320	0.15	0.089	1.64	1150
Diesel	850	660	1.9	300	0.15	0.098	3.35	1100
Diesel [21]	–	–	–	–	–	–	–	1100
Ethanol	785	351	2.57	846	0.16	0.082	0.98	1350
Ethanol [22]	–	–	–	–	–	–	–	1310

4. The computational procedure

The equations described above are set out in a MATLAB code called *M-pan-burn* to obtain mass loss vs. time result for a given set of parameters. For specific calculations, fuel initial temperature, T_0, the fuel thickness, h_{fu} are required to be set.

The flame temperature – time behaviour that includes the initial ignition transient is the input for the gas phase flux as well as wall conduction. The gas phase temperature with time is simulated through an expression that allows for random fluctuations. It is taken as

$$T_f = T_0 + (1200 - T_0)[1 - \exp(-t/5)] + C_4[\sin(\pi t/30 + tR(t)] \tag{42}$$

where C_4 is a constant taken here as 15 and $R(t)$ is a random function of value between 0 and 1. Increase in C_4 implies larger fluctuation is gas phase temperature. The gas phase flux fluctuates like-wise, with fluctuations in radiation flux being much larger. The c-phase dynamics controlled by the slow conduction process averages the fluctuation. After trials and examination of experimental data it was thought adequate to take the value as indicated. Then, c_{Tp} is calculated from Equation (25) and Equation (18) is treated to get $\mathrm{d}T_p/\mathrm{d}t$. With a time step taken as 1 s here the calculation of T_p is advanced. Then, Equation (19) is solved to get T_{wbc}. Following this, T_{w1} and T_{wb} are calculated from Equation (21). Using

the heat transfer coefficients, $h_{g,\mathrm{conv}} = 0.0045\,\mathrm{kW/m^2K}$ and Equations (28)–(30), $h_{g-w,fu}$ is obtained. These are used then to calculate convective and conductive fluxes from (9) and (26). Radiation flux is calculated from Equation (13). These are summed up to get the total flux, $\dot{q}''_{tot}$. Both the surface temperature, T_s and the bottom liquid temperature, T_{bot} are then calculated using Equation (41). When both surface and in-depth temperatures reach boiling point they are set at the boiling point. It must be pointed out that even though the radiation flux depends on the burn flux which itself is not known, the calculation is performed in an explicit mode by providing an arbitrary small value to begin with and proceeding forward at each time with the previous values. Since the changes that occur are slow compared to the chosen time step (1 s) and is controlled by convection in the early part, this approach is considered satisfactory.

These are then used in the heat balance equation to get the fuel mass flux as

$$\dot{m}''_{\mathrm{fu}} = \frac{\dot{q}''_{\mathrm{tot}}}{L_{\mathrm{fu}} + c_{p,fu}(T_{bfu} - T_{\mathrm{bot}})} \tag{43}$$

With the information on the fuel mass flux, the amount consumed in the time step and amount remaining are obtained. The process is repeated till burnout – the mass remaining goes below a small fraction – 1 % in the code *M-pan-burn*. The operational code containing the above discussed model to capture the fuel depth, pan material and pan diameter effect on the mass burn rate of pan fires is made available in the web page https://www.jainuniversity.ac.in/FCRC/research-fcrc as model to predict the mass burn rate of pool fires (*M-pan-burn*).

5. Results and discussion

Predictions over 75 different cases covering the range of materials, fuel depth and pan diameter have been obtained. We show the results for n-heptane in this section and for other fuels in the next section.

5.1. *n-heptane*

Comparisons of predictions are shown for experiments of Refs. [11, 16, 17, 18, 23, 24]. Also the role of various components of flux as a function of pan diameter and fuel depth are discussed. In so far predictions are concerned, mean burn flux (or total burn time), fuel mass vs. time behaviour and the tip wall temperature are in the order of importance. Since the data set is large, only illustrative cases are presented here. Detailed comparison shows it to be outstanding for 35 cases, moderate for 25, poor for about 5. It is not that comparisons cannot be made better in the small number of cases, but would require specific tuning, something that is not contemplated here because it would not add value if the code has to be used in a predictive mode. The code output has a result on $\bar{\dot{m}}''_{\mathrm{fu}}$ from the correlation (see Shiva kumar et al. [16]), from the unsteady code itself, their mean and the deviation of this value from experimental result. Since the code has also approximations due to the choice of the constants c_{Tp} and C_3 which depend on the dimensionless parameters, there will also be inaccuracies in the results. The choice of a mean value is intended to average out these inaccuracies. However, in some cases, the experimental value is closer to that from either the correlation or the code and has a larger deviation from the mean.

Figure 5 shows the comparison of mass vs. time for 0.2 m pans made of Aluminum, MS, SS and Glass with fixed fuel depth of 13 mm. The quality of mass vs. time prediction

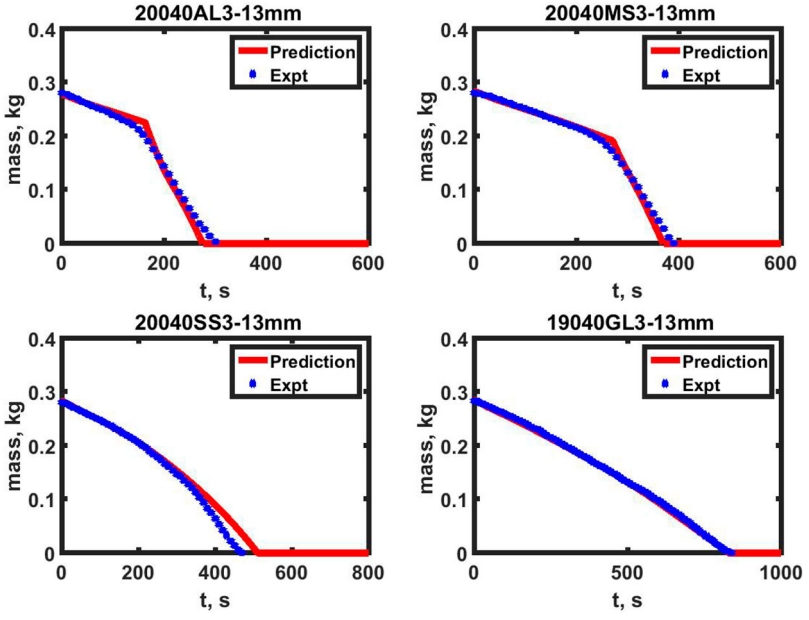

Figure 5. Comparison between code predictions and experimental data on mass vs. time for Aluminum (Al), Mild steel (MS), Stainless Steel (SS) (all 200 mm dia) and glass (GL), 190 mm dia at a fuel depth of 13 mm (20040AL3-13 mm implies 200 mm dia, 40 mm depth Aluminum pan of 3 mm thick with 13 mm n-heptane fuel depth).

seems outstanding for all the cases. As can be noted, MS and AL pans belonging to sharp transition (type I) and SS and GL show smooth variation (type I) and the comparison between predictions and experiments is good. In the case of glass the flux does not deviate much indicating that conduction and radiation are playing little role in the burn process.

Figure 6 presents the results of mass vs. time comparisons between code and experiments for MS pan as a function of depth at 10, 13, 20 and 30 mm. The quality of predictions seems reasonable to very good in terms of burn time. It is useful to bring out that the break in slope has a relationship with the non-dimensional quantities through relationships (31) and (32) as well as (33) and (34). Figure 7 shows the comparison of mass vs. time for the experiments performed at different initial temperatures by Chen et al. [18, 19] and Kang et al. [23] in a 0.2 m diameter pan. The comparison is impressive considering that the data at 343 K is close to the boiling point (369 K). Differences in the tail-off zone are due to minor wind effects at the end. Comparisons of pressure effects on burn flux for the data from Li et al. [11] shown in Figure 8 appears moderately good. As can be noted that the code is able to capture the effect of pressure on the mass loss rate considering the fact that Ditch et al. [7] had expressed concerns regarding the experimental data in relationship to their correlation.

Figure 9 shows the comparison of mass vs. time for pan diameters of 0.2, 0.3, 0.5 and 2 m. As can be noted the diameter effect is captured very well particularly at large depths where the burn flux attains large values (65 g/m^{2}s) comparable to large diameter pans.

We turn our attention to predictions of pan tip temperature. Figure 10 shows comparison of experimental and predicted pan tip temperature by the code for AL, MS, SS and GL pan with 13 mm fuel depth, as the pan tip temperature is one of the important parameter that

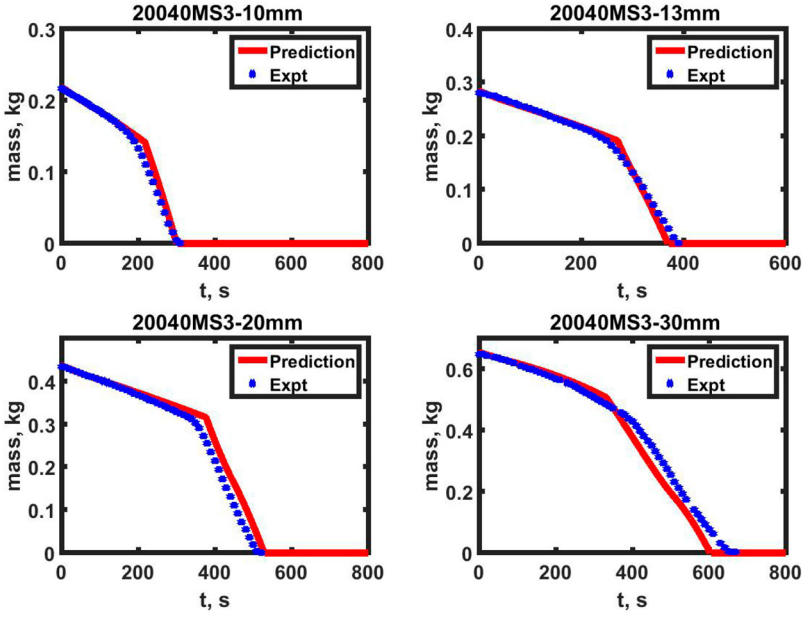

Figure 6. Comparison between code predictions and experimental data on mass vs. time for MS pan 0.2 m dia, 40 mm deep for fuel depths of 10, 13, 20 and 30 mm (20040MS3-10 mm implies 200 mm dia, 40 mm depth mild steel pan of 3 mm thick with 10 mm n-heptane fuel depth).

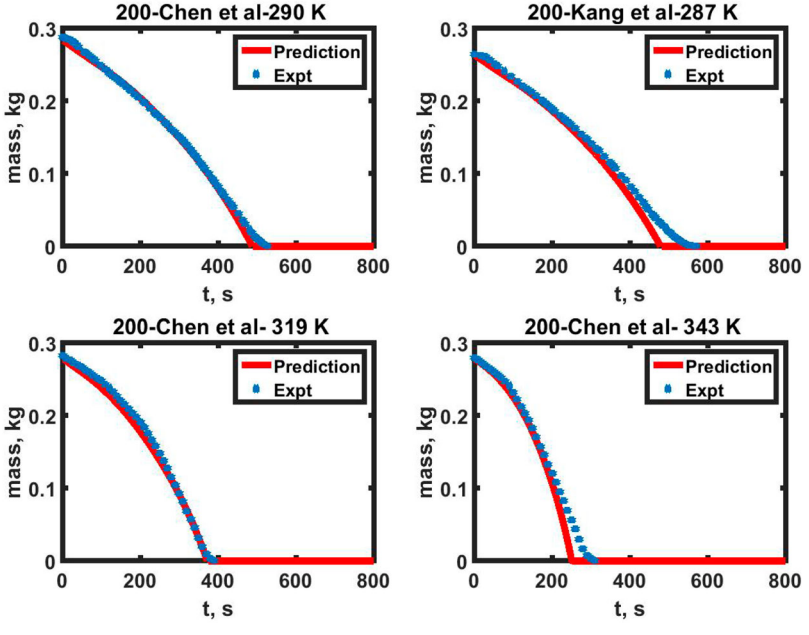

Figure 7. Comparison between code predictions and experimental data on mass vs. time for the experiments of Chen et al. [18, 19] and Kang et al. [23] performed in 0.2 m diameter pan at different initial temperatures for n-heptane fuel (200-Chen et al-290 K implies 200 mm diameter pan of Chen et al at initial temperature of 290 K).

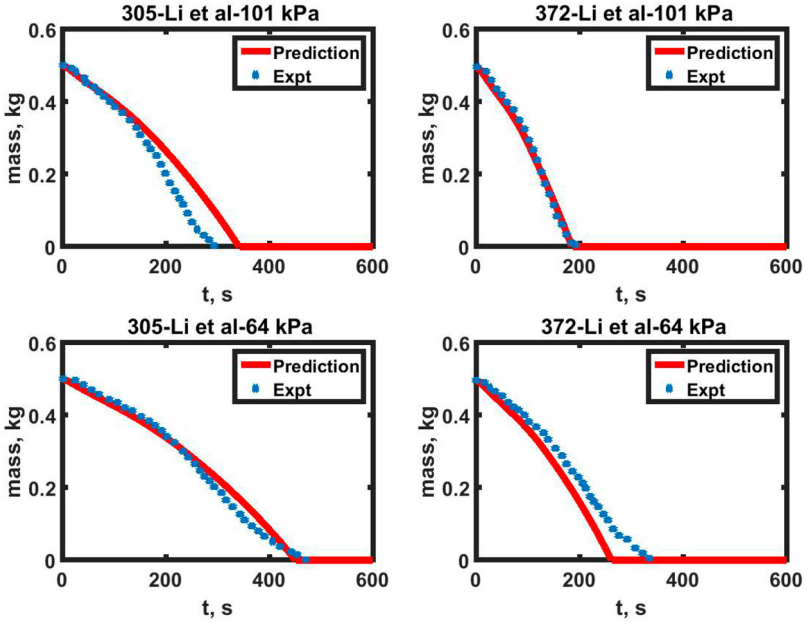

Figure 8. Comparison between code predictions and experimental data on mass vs. time for the experiments of Li et al. [11] performed in 0.305 and 0.372 m diameter pans at different atmospheric pressures for n-heptane (305-Li et al-101 kPa implies 305 mm dia pan of Li et al. at 101 kPa pressure).

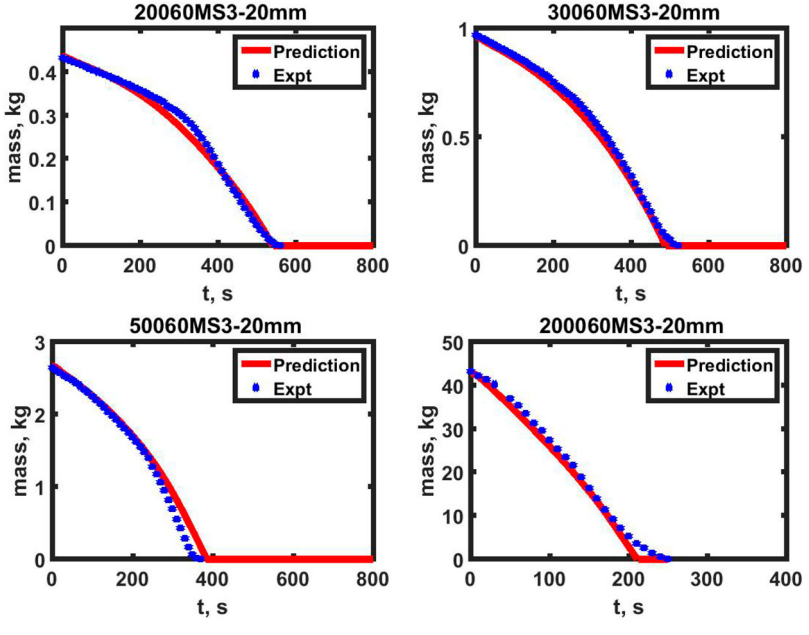

Figure 9. Comparison between code predictions and experimental data on mass vs. time for MS pans, 60 mm deep for pans of 0.2, 0.3, 0.5 and 2 m diameter with n-heptane fuel (20060MS3-20 mm implies 200 mm dia 60 mm depth mild steel pan of 3 mm thick with 20 mm fuel).

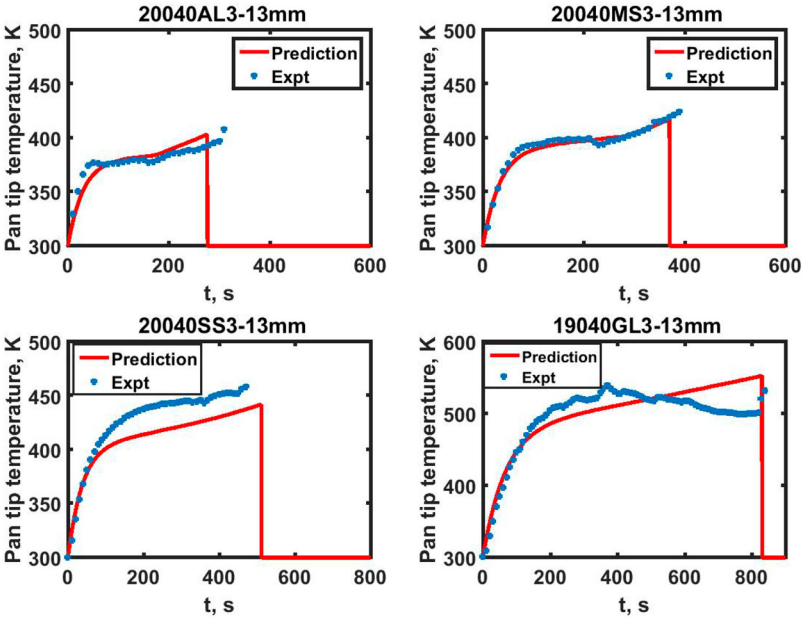

Figure 10. Comparison between code predictions and experimental data on pan tip temperature for AL,MS, SS and GL pan for n-heptane fuel depth of 13 mm.

aids in precise modelling of the wall conductive heat flux into the fuel. The predictions are reasonable-to-good for the cases whose data are set out. In the case of glass, the prediction shows a growing trend and the data shows that it has stabilised at around 530 K much earlier. This is conjectured to be due to the fact that there will be radiant losses and free convective losses due to flow of air around the pan not accounted for in the model.

The magnitude of the fluxes for different wall materials for several cases are set out in Figure 11. Convective flux is about 4 kW/m^2 for all the cases. Radiative flux increases with burn because the mass flux is increasing and the peak flux values are close to 65 g/m^{2}s. Conductive flux increases through the burn very significantly for SS, and MS pans. The peak flux values for MS and GL are 24 and 5 kW/m^2 (for SS it is about 9 kW/m^2, not shown here). It is the conductive flux contribution that leads to the observed behaviour in small pans. While the fraction of conductive flux is more than 35% for metals, its is about 10% for glass. As can be seen the role of radiation gets enhanced with increasing diameter.

5.2. *Other fuels – diesel, kerosene and ethanol*

Figures 12 and 13 show the comparison of experimental and the predicted mass burn rate for the kerosene and diesel fuels in 0.2 m diameter MS and SS pans with the choice of parameters outlined in Tables 1 and 2. As can be noted that the results of the code can be see to capture the burn behaviour of diesel better than kerosene. What appears interesting is that even though there are numerical differences, some variations are also tracked (see 20040SS-10 mm-Kerosene case). Figure 14 shows the comparison of experimental and code predictions for 0.2 m diameter MS pan with ethanol at fuel depths of 10 and 20 mm and from the figure it is evident that the code is able to capture the burn behaviour of alcohols as well.

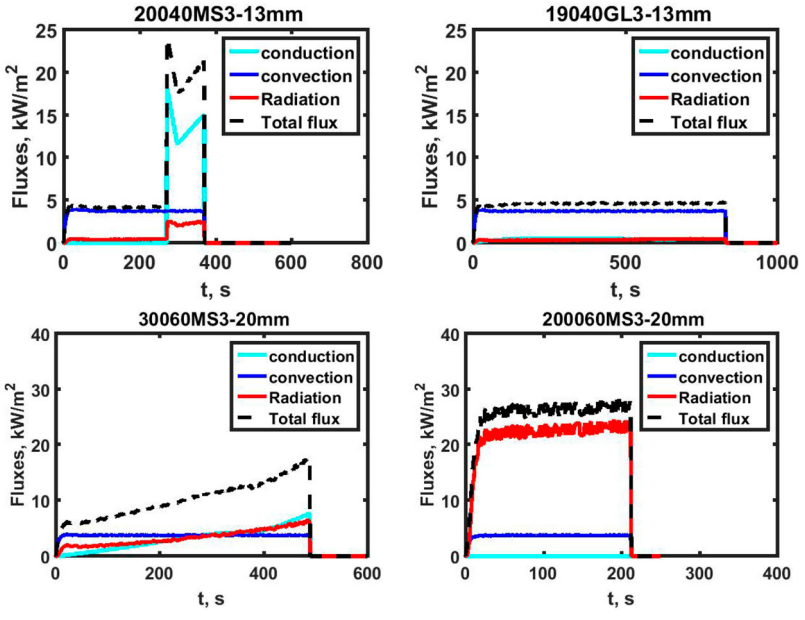

Figure 11. The variation of convective, radiative and conductive fluxes for MS and GL pans of 0.2 m diameter and 0.3 m and 2 m diameter pans with n-heptane fuel.

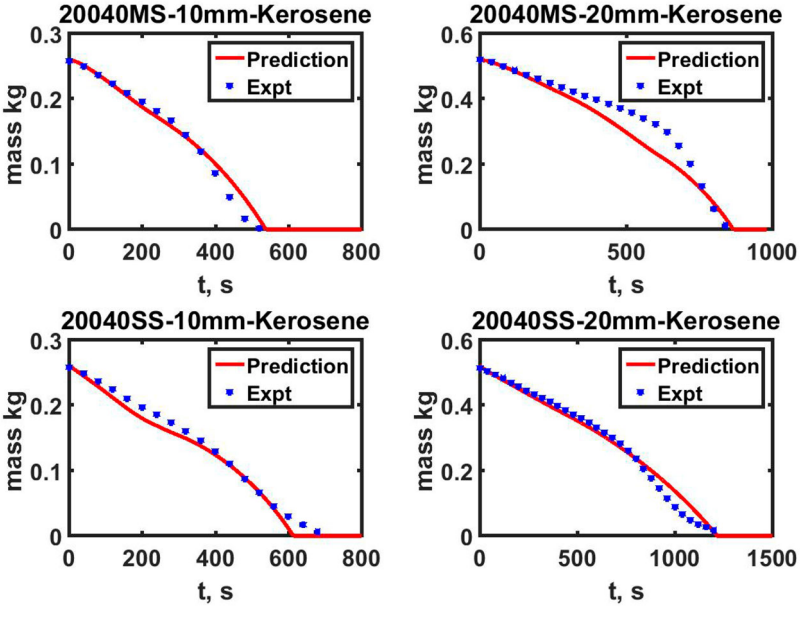

Figure 12. Comparison between code predictions and experimental data on mass burn data of kerosene fuel for MS and SS pans at fuel depths of 10 and 20 mm.

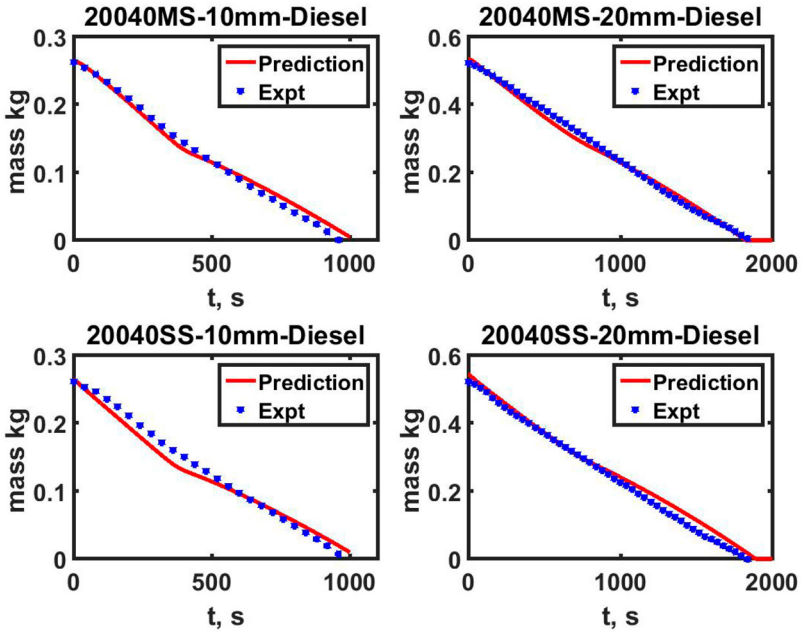

Figure 13. Comparison between code predictions and experimental data on mass burn data of diesel fuel for MS and SS pans at fuel depths of 10 and 20 mm.

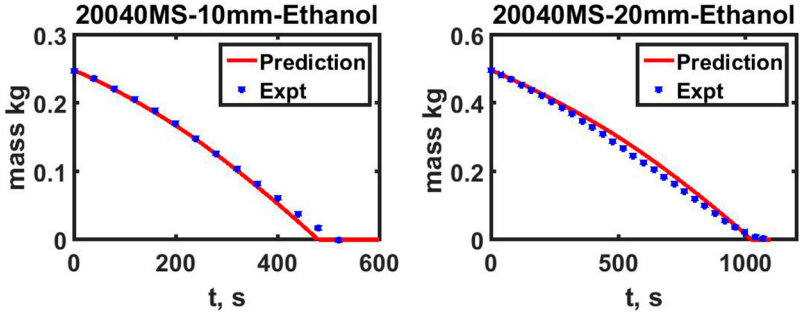

Figure 14. Comparison between code predictions and experimental data on mass burn data of ethanol fuel for MS pan at fuel depths of 10 and 20 mm.

Table 3 presents the results of comparisons between predictions and experiments on mean mass flux for over some conditions with three data from references [19, 24]. In these tables, $Pred_1$ is obtained from the correlation [16] and $Pred_2$ is obtained from the MATLAB code. An average between $Pred_1$ and $Pred_2$ constitutes the prediction and is compared with the experimental result. The experimental accuracy is set at $\pm$ 5%. Where the prediction and experimental value differ by less than 5%, the difference is considered negligible. There are cases where the error is much larger. In several of these cases, the comparative mass vs. time plot shows that the prediction follows the experimental variation quite accurately till late into the burn and deviates only beyond that stage. It is inferred that

Table 3. $\bar{m}''_{fu}$ (g/m^{2}s) for 0.2 m dia pans of different materials with different freeboard values and initial temperatures; Expt, $Pred_1$, $Pred_2$, Mean, % Error; negble = error is less than experimental accuracy $\sim$ 5 %, SS-CK of Chen et al. [19] and Kang et al. [23].

Matrl	h_{pan} m	h_{fu} m	h_{fb} m	T_0 K	Expt g/m^{2}s	$Pred_1$ g/m^{2}s	$Pred_2$ g/m^{2}s	Mean g/m^{2}s	% Error –
MS	0.04	0.010	0.030	300	21.9	20.8	21.0	20.9	negble
MS	0.04	0.013	0.027	300	22.7	22.8	22.7	22.7	negble
MS	0.04	0.020	0.020	300	26.2	26.5	26.0	26.2	negble
MS	0.06	0.010	0.050	297	19.4	18.0	20.6	19.4	negble
MS	0.06	0.030	0.030	300	27.6	24.2	27.4	25.8	negble
MS	0.06	0.040	0.020	300	27.2	24.5	28.6	26.5	negble
SS-CK	0.04	0.012	0.028	288	15.1	17.6	17.2	17.4	+ 13
SS-CK	0.04	0.013	0.027	365	46.0	64.6	43.0	53.8	+ 17

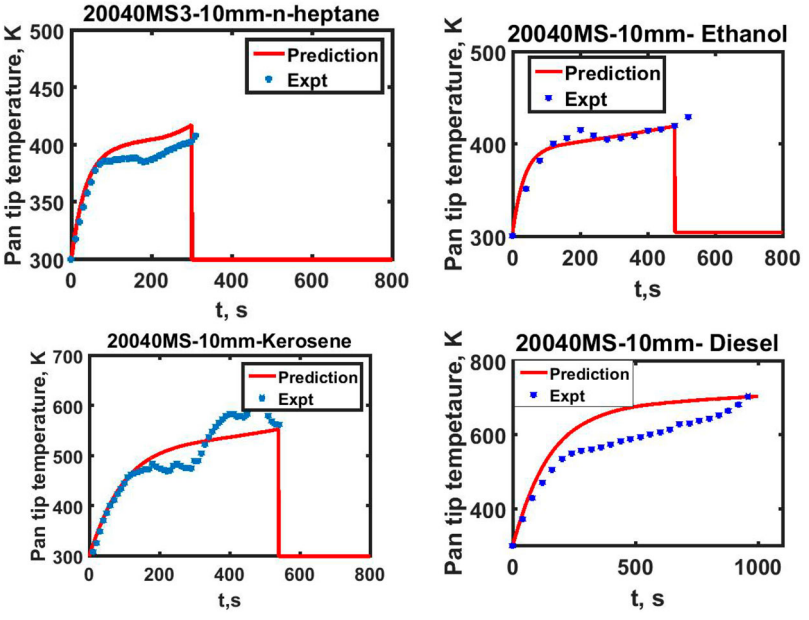

Figure 15. Comparison between predictions and experiments on pan tip temperatures for 0.2 dia, MS pan with 10 mm fuel depths of n-heptane, ethanol, kerosene and diesel.

all the effects namely diameter, wall conductivity, and free board are captured reasonably well.

The study of how the temperature in the liquid phase behaves, the data on the temperatures of the liquid at 1 mm from the bottom have been discussed in [17]. It was shown that for pure fuels like n-heptane and ethanol, the temperature reaches their respective boiling points and stays at that temperature till complete burnout occurs. In the case of kerosene and diesel, the temperature keeps on increasing with time till the end of the experiment, since they are fuels composed of various petroleum fractions. In the case of diesel, the temperatures go beyond 650 K indicating to evaporation of some heavy fragments in the fuel.

Table 4. $\bar{\dot{m}}''_{fu}$ (g/m^{2}s) for 0.05, 0.1, 0.141 m dia SS (C-K = Chen and Kang [19, 23] SS [18] and GL-Glass pans.

d_{pan} m	h_{pan} m	h_{fu} m	h_{fb} m	T_0 K	Expt g/m^{2}s	$Pred_1$ g/m^{2}s	$Pred_2$ g/m^{2}s	Mean g/m^{2}s	% Error –
0.141	0.04	0.013	0.027	278	14.0	14.5	15.3	14.9	negble
C-K	0.04	0.013	0.027	290	15.2	15.2	15.6	15.4	negble
	0.04	0.013	0.027	319	18.1	18.0	19.0	18.5	negble
0.10	0.04	0.013	0.027	290	12.4	13.9	15.3	13.4	− 9
C-K	0.04	0.013	0.027	319	13.4	16.3	15.1	15.5	+ 13
0.1	0.04	0.010	0.030	300	15.8	14.2	16.2	15.1	negble
Present	0.04	0.013	0.027	300	15.8	14.1	12.4	13.2	− 12
0.05 [24]	0.11	0.110	0.000	298	16.9	7.9	16.5	12.2	− 27

Figure 15 shows the plots of pan tip temperatures for various fuels for 0.2 m dia pan at 10 mm fuel depth. As can be noted, the comparisons for kerosene and diesel can be considered average due the actual property variation through the burn being not accounted. While improvements may be possible, they are not considered warranted at this stage.

5.3. *Pans of diameter < 0.2 m*

Hayasaka [24] and Chen et al. [18, 19] have experimented upon SS pans of 0.05, 0.1 and 0.141 m diameter. Experiments were conducted here for comparison purposes with SS (ours) and glass for 0.1 m diameter. The predictions made using *M-Pan-burn* are set out in Table 4. Here again the predictions seem not unreasonable if we note that the methodology followed is the same as for larger diameter pans.

6. Concluding remarks

Noting that non availability of mathematical model that captures the time varying behaviour of pool fire in the literature, the study was initiated and a mathematical model to calculate the burn rate in an unsteady pan fire considering all the controlling geometric, thermodynamic and transport properties was developed and named as *M-Pan-burn* using MATLAB software.

A MATLAB code that calculates the instantaneous burn rate flux using the modelled heat flux from the various components, convection, conduction and radiation has been set. The convective heat transfer coefficient of 0.0045 $p^{2/3}$ kW/m^2 K has been found valid over all the pan and fuel parameters discussed here. The model for radiation is different from what has been in the literature as it had to account for enhanced burn flux due in part due to radiation something not accounted for in earlier models. This model uses fire emissivity and a view factor both of which have diameter dependences. The maximum temperature at which radiation occurs is based on a measured mean fire temperature (the mean of the maximum values measured at the centreline of pool fire for a certain duration of time) and it varies between 1100 and 1350 K depending on the fuel. This choice of temperatures is assumed to account for all the chemistry effects influencing the heat release process. Wall conduction modelling invokes experimental features, namely the initial temperature rise rate that appears to be independent of pan material and fuel depth, a near-linear temperature variation along the wall and the fact that all the heat transfer along the wall appears at

the centre of the pan after it transfers the heat to the liquid. This heat transferred raises the bottom temperature in time as it cannot achieve steady state. Three dimensionless numbers $Mpc1$, W and W_1 are set out to evolve a correlation for the three important constants, C_2, c_{Tp} and C_3 in the model with c_{Tp} controlling the peak wall tip temperature, C_2, and C_3 controlling the heat transfer by convection into the liquid. The liquid heat transfer is treated unsteady with dependence on the fuel thermal diffusivity and its parameter of the dimensionless temperature variation are derived by comparison with experimental data. These features are integrated into the code *M-Pan-burn* that needs the wall and fuel thermal property data as well as initial fuel depth and temperature as inputs to predict the burn behaviour. It must be emphasised that there are no free constants in the code to make predictions. The results of this code show that the predicted burn behaviour follows the experimental burn profile nearly exactly in several cases and provides the magnitude of various components of heat flux with time. The conductive flux varies with time something that could have been anticipated, but obtained only by using an unsteady code of the kind described here.

Mean burn flux values are obtained as an average between that from the correlation and the code and presented as the final result for the mean burn flux. The comparison with the experimental results is excellent-to-good in most cases. Where there is a departure, it turns out that the predicted burn profile matches with that from experiment for the early part of the burn and the deviation occurs later. One of the important uses of the code would be to deploy it for incremental parameter influences since it will be more accurate than predictions for a new set of parameters. The code presented here can be used for the open pool fires and possible extension of the code to pool fires in enclosures and wind are being actively pursued.

Acknowledgments

The authors are thankful to the authorities of Jain (Deemed-to-be-university) for encouragement in the conduct of this research.

Disclosure statement

No potential conflict of interest was reported by the author(s).

References

[1] H.C. Hottel, *Review: Certain laws governing diffusive burning of liquids*, Fire Res. Abstr. Rev. 1 (1958), pp. 41–44.
[2] J.P. Spinti, J.N. Thornock, E.G. Eddings, P.J. Smith, and A.F. Sarofim, *Heat transfer to objects in pool fires*, Chapter 6 in *Transport Phenomena in Fires*, M. Fagri and B. Sunden, eds., WIT Press, USA, 2008, pp. 67–127.
[3] A. Hamins, S.J. Fischer, T. Kashiwagi, M.E. Klassen, and J.P. Gore, *Heat feed back to the fuel surface in pool fires*, Combust. Sci. Technol. 97 (1994), pp. 37–62.
[4] C.C. Ndubizu, D.E. Ramaker, P.A. Tatem, and F.M. Williams, *A model for free burning fires*, Combust. Sci. Technol. 31 (1983), pp. 233–247.
[5] J. de Ris and L. Orloff, *A dimensionless correlation of pool burning data*, Combust. Flame.18 (1972), pp. 381–388.
[6] L. Orloff and J. de Ris, *Froude modeling of pool fires*, Symp. (Int.) Combust. Flame. 19 (1982), pp. 885–895.

[7] B.D. Ditch, J. de Ris, T.K. Blanchet, M. Chaos, G.B. Robert, Jr., and S.B. Dorofeen, *Pool fires – an empirical correlation*, Combust. Flame. 160 (2013), pp. 2964–2974.
[8] V. Babrauskas, *Estimating large pool fire burning rates*, Fire Technol. 19 (1983), pp. 251–261.
[9] J.M. Chatris, J. Quintela, J. Folch, E. Planas, J. Arnaldos, and J. Casal, *Experimental study of burning rate in hydrocarbon pool fires*, Combust. Flame. 126 (2001), pp. 1373–1383.
[10] M. Munoz, E. Planas, F. Ferrero, and J. Casal, *Analysis of the geometric and radiative characteristics of hydrocarbon pool fires*, Combust. Flame. 139 (2004), pp. 263–277.
[11] Z. Li, Y. He, H. Zhang, and J. Wang, *Combustion characteristics of n-heptane and wood crib fires at different altitudes*, Proc. Comb. Inst. 32 (2009), pp. 2481–2488.
[12] J. Fang, R. Tu, J. Guan, J. Wang, and Y. Zhang, *Influence of low air pressure on combustion characteristics and flame pulsation frequency of pool fires*, Fuel 90 (2011), pp. 2760–2766.
[13] J. de Ris, A.M. Kanury, and M.C. Yuen, *Pressure modeling of fires*, 14th Symp. Combustion. 14 (1973), pp. 1033–1044.
[14] D. Wieser, P. Jauch, and U. Willi, *The influence of high altitude on fire detector test fires*, Fire Safe J. 29 (1997), pp. 195–204.
[15] R.L. Alpert, *Pressure modeling of fires controlled by radiation*, Proc. Combust. Inst. 16 (1976), pp. 1489–1500.
[16] A. Shiva kumar, A.Ve. Sowriraajan, C.S. Bhaskar Dixit, and H.S. Mukunda, *Experiments on unsteady pool fires – effects of fuel depth, pan size and wall material*, Sadhana, Indian Acad. Sci. 46 (2021).
[17] A. Shiva kumar, H.S. Mukunda, and C.S. Bhaskar Dixit, *Effects of fuel depth and pan wall material for unsteady pool fires with different fuels*, Fire Technol. (2021).doi:10.1007/s10694-021-01159-1.
[18] B. Chen, S. Lu, C. Li, Q. Kang, and V. Lecoustre, *Initial fuel temperature effects on burning rate of pool fire*, J. Hazard Mater. 188 (2011), pp. 369–374.
[19] B. Chen, S. Lu, C. Li, Q. Kang, and M. Yuan, *Unsteady burning of thin layer pool fires*, J. Fire Sci.30 (2011), pp. 3–15.
[20] J.G. Quintiere, *Fundamentals of fire phenomena*, John Wiley and Sons, USA, 2006, pp. 138–154.
[21] S. Sudheer and S.V. Prabhu, *Measurement of flame emissivity of hydrocarbon pool fires*, Fire Technol. 48 (2012), pp. 183–217.
[22] E.J. Weckman and A.B. Strong, *Experimental investigation of the turbulence structure of medium scale methanol pool fires*, Combust. Flame 105 (1996), pp. 245–266.
[23] Q. Kang, S. Lu, and B. Chen, *Experimental studies on burn rate of small scale heptane pool fires*, Eng. Thermophys. Chinese Sci. Bull. 55 (2010), pp. 973–979.
[24] H. Hayasaka, *Unsteady burning rates of small pool fires*, Symp. (Int.) Fire Saf. Sci. 5 (1997), pp. 499–510.